Received: 25 December 2022 | Revised: 22 March 2023 | Accepted: 10 April 2023

DOI: 10.1111/liv.15587

Liver INTERNATIONAL WILEY

ORIGINAL ARTICLE

Long-term hypercaloric diet exacerbates metabolic liver disease in PNPLA3 I148M animals

Huan Su[1] | Madhuri Haque[1] | Svea Becker[1] | Karolina Edlund[2] | Julia Duda[3] | Qingbi Wang[1] | Johanna Reißing[1] | Hanns-Ulrich Marschall[4] | Lena S. Candels[1] | Mohamed Mohamed[1] | Wilhelm Sjöland[4] | Lijun Liao[5] | Stephan A. Drexler[1] | Till Strowig[6] | Jörg Rahnenführer[3] | Jan G. Hengstler[2] | Maximilian Hatting[1] | Christian Trautwein[1]

[1]Department of Medicine III, University Hospital RWTH Aachen, Aachen, Germany

[2]Department of Toxicology, Leibniz Research Centre for Working Environment and Human Factors, Technical University Dortmund, Dortmund, Germany

[3]Department of Statistics, TU Dortmund University, Dortmund, Germany

[4]Department of Molecular and Clinical Medicine, University of Gothenburg, Gothenburg, Sweden

[5]Department of Pain Management, Shanghai East Hospital, School of Medicine, Tongji University, Shanghai, China

[6]Helmholtz Centre for Infection Research, Braunschweig, Germany

Correspondence
Maximilian Hatting, MD and Christian Trautwein MD, Professor of Medicine, Department of Medicine III, University Hospital RWTH Aachen, Pauwelsstraße 30, Aachen 52074, Germany.
Email: ctrautwein@ukaachen.de and max.hatting@live.com

Abstract

Background & Aims: Nonalcoholic fatty liver disease (NAFLD) is a major health burden associated with the metabolic syndrome leading to liver fibrosis, cirrhosis and ultimately liver cancer. In humans, the PNPLA3 I148M polymorphism of the phospholipase patatin-like phospholipid domain containing protein 3 (PNPLA3) has a well-documented impact on metabolic liver disease. In this study, we used a mouse model mimicking the human PNPLA3 I148M polymorphism in a long-term high fat diet (HFD) experiment to better define its role for NAFLD progression.

Methods: Male mice bearing wild-type *Pnpla3* (*Pnpla3*^{WT}), or the human polymorphism PNPLA3 I148M (*Pnpla3*$^{148M/M}$) were subjected to HFD feeding for 24 and 52 weeks. Further analysis concerning basic phenotype, inflammation, proliferation and cell death, fibrosis and microbiota were performed in each time point.

Results: After 52 weeks HFD *Pnpla3*$^{148M/M}$ animals had more liver fibrosis, enhanced numbers of inflammatory cells as well as increased Kupffer cell activity. Increased hepatocyte cell turnover and ductular proliferation were evident in HFD *Pnpla3*$^{148M/M}$ livers. Microbiome diversity was decreased after HFD feeding, changes were influenced by HFD feeding (36%) and the PNPLA3 I148M genotype (12%). *Pnpla3*$^{148M/M}$ mice had more faecal bile acids. RNA-sequencing of liver tissue defined an HFD-associated signature, and a *Pnpla3*$^{148M/M}$ specific pattern, which suggests Kupffer cell

Abbreviations: ALT, alanine aminotransferase; AST, aspartate transaminase; BAs, bile acids; BMI, body mass index; Ccl2, CC-chemokine ligand 2; CCL5, chemokine (C-C motif) ligand 5; Ccr1, chemokine (C-C motif) receptor 1; Ccr2, chemokine (C-C motif) receptor 2; Ccr5, chemokine (C-C motif) receptor 5; CK19, cytokeratin-19; Clec4f, C-Type Lectin Domain Family 4 Member F; CGI-58, Comparative gene identification-58; CYP7A1, cytochrome P450 family 7 subfamily A member 1; DNL, de novo lipogenesis; Ephb2, Eph receptor B2; GO, gene ontology; HFD, high fat diet; HSCs, hepatic stellate cells; HTGC, hepatic triglyceride content; LDA, Linear discriminant analysis; LPAAT, Lysophosphatidic acid acyltransferase; NAFLD, nonalcoholic fatty liver disease; NASH, nonalcoholic steatohepatitis; NTCP, sodium taurocholate co-transporting polypeptide; OTUs, Operational Taxonomic Units; Pilra, paired immunoglobin-like type 2 receptor alpha; PNPLA3, patatin-like phospholipid domain containing protein 3; Spp1, secreted phosphoprotein 1; SREBP-1c, sterol regulatory element binding protein 1c; Timp1, tissue inhibitor of metalloproteinase 1; TGs, Triglycerides; Vcan, versican; WT, wild type.

Maximilian Hatting and Christian Trautwein are shared senior authors.

Funding information
Deutsche Forschungsgemeinschaft CRC1382, Grant/Award Number: 403224013; Deutsche Forschungsgemeinschaft, Grant/Award Number: HA 7246/2–1 and Tr 285/10–2

Handling editor: Luca Valenti

and monocytes-derived macrophages as significant drivers of liver disease progression in *Pnpla3*$^{148M/M}$ animals.

Conclusion: With long-term HFD feeding, mice with the PNPLA3 I148M genotype show exacerbated NAFLD. This finding is linked to PNPLA3 I148M-specific changes in microbiota composition and liver gene expression showing a stronger inflammatory response leading to enhanced liver fibrosis progression.

KEYWORDS
Kupffer cells, liver chronic inflammation, liver fibrosis, NAFLD

1 | INTRODUCTION

The metabolic syndrome linked to non-alcoholic fatty liver disease (NAFLD) is becoming increasingly relevant due to its widespread occurrence in all populations, particularly among those with a sedentary lifestyle. In addition to lifestyle and nutrition, genetic risk factors play a major role for the progression of NAFLD, of which the patatin-like phospholipid domain containing protein 3 (PNPLA3) I148M polymorphism is of major relevance. In Caucasian populations, this polymorphism has an allele frequency of 0.28. Homozygote allele carriers have a 3.3-fold increased incidence of nonalcoholic steatohepatitis (NASH) and liver fibrosis in a European cohort.[1,2]

PNPLA3 I148M mutation has been shown to be associated with increased hepatic lipids accumulation.[3] Li et al. found increased triglycerides (TGs) synthesis in mice expressing human PNPLA3 I148M.[4] Conversely, the hepatic de novo lipogenesis (DNL) was lower in a human PNPLA3 I148M cohort.[5] Moreover, the sterol regulatory element binding protein 1c (SREBP-1c) which is the key enzyme for DNL was decreased.[5] Additionally, it was reported that the PNPLA3 I148M variant protein showed less lipase activity especially the lysophosphatidic acid acyltransferase (LPAAT) effect.[6,7] Wang et al. also reported that PNPLA3 I148M together with comparative gene identification-58 (CGI-58) would inhibit adipose triglyceride lipase on lipid droplet.[8] Therefore, it is more reasonable to assume that the PNPLA3 I148M mutation leads to a loss of function, thereby exacerbating disease progression.

Fibrogenesis, as a hall marker for NAFLD, could be accelerated by the PNPLA3 I148M mutation directly or indirectly. In wild type mice, PNPLA3 protein has a protective role, can promote retinoids release from hepatic stellate cells (HSCs), which may decrease extracellular matrix formation and remodelling. However, when the PNPLA3 I148M mutation is present, this function was lost.[9] On the other hand, under liver injury, HSCs can release inflammatory cytokines and trigger stronger inflammation, which in turn promotes fibrosis. Primary human HSCs with the PNPLA3 I148M polymorphism were shown to release higher levels of proinflammatory cytokines such as chemokine (C-C motif) ligand 5 (CCL5).[10] During this process, monocyte derived macrophages and liver resident Kupffer cells play a key role in releasing proinflammatory mediators and activate myofibroblasts.[11] However, it is poorly understood how PNPLA3 I148M influences the function of macrophages and Kupffer cells.

Key points

PNPLA3 I148M polymorphism triggered stronger inflammation, apoptosis and fibrosis in mice liver under long-term high fat diet experiment. RNA-Sequencing revealed a cluster of genes increase macrophages and Kupffer cells infiltration and thus promote the disease progression.

Furthermore, related genes or pathways activated specifically by the PNPLA3 I148M genotype are not fully understood.

Nevertheless, obesity is essential to amplify the impact of the PNPLA3 I148M genotype on hepatic triglyceride content (HTGC) and liver damage. In a lean population with a body mass index (BMI) of lower than 25 kg/m^2, wild-type(I148I) or I148M homozygous individuals have similar levels of HTGC and AST. In contrast, PNPLA3 I148M homozygous carriers show significantly higher HTGC and AST levels compared to the wild type, when an increased BMI is present.[12] In addition, I148M homozygous individuals are more frequent among obese individuals who also have a higher likelihood to develop the metabolic syndrome.[13]

The current study aims to define the impact of the PNPLA3 I148M genotype on NAFLD especially in obese and older animals after long-term hypercaloric feeding. We here define that PNPLA3 I148M-specific changes in gene signature and microbiota composition is associated with stronger monocyte-derived inflammation and liver disease progression in NAFLD.

2 | MATERIALS AND METHODS

2.1 | Animals

PNPLA3 I148M knock-in (KI; *Pnpla3*$^{148M/M}$) mice were generated with genetically modified embryonic stem cells in which the codon for Isoleucine 148 (ATT) was replaced by Methionine codon (ATG).[14,15] *Pnpla3*^{WT} and *Pnpla3*$^{148M/M}$ animals were both on a C57Bl/6J mice background. Before starting the experiments both animals were intercrossed and heterozygote *Pnpla3*^{WT}/*Pnpla3*$^{148M/M}$ animals were generated. These mice were intercrossed to generate *Pnpla3*^{WT},

Pnpla3$^{148M/M}$ and *Pnpla3*^{WT}/*Pnpla3*$^{148M/M}$. *Pnpla3*$^{148M/M}$ and *Pnpla3*^{WT} (*Pnpla3*$^{+/+}$) mice of male gender were housed in the Central Animal Facility University Hospital RWTH Aachen with a 12/12-h light/dark cycle and free access to food and water. All mice were fed with standard chow diet (V1534-300, Ssniff) until 8–10 weeks old and started with diet experiments. The chow diet group was fed with the standard chow diet while the HFD group changed to a 40 kcal% fat, 20 kcal% fructose and 2% cholesterol diet (D09100308, RESEARCH DIETS Inc.) for 24 and 52 weeks. The mice were set to fast for 3 h before sacrifice. Animal experiments were performed in accordance with the criteria of the German administrative panels on laboratory animal care and approved by the local Animal Care Committees (#AZ-84-02.04.2016.A443).

2.2 | Methods

Microbiota samples were analysed by 16 s RNA sequencing (Helmholtz Centre for Infection Research). RNA-Sequencing of liver tissue was performed at the Leibniz Research Centre for Working Environment and Human Factors (IfADo) at the TU Dortmund as previously described.[16] Bile acids were investigated by ultra-performance liquid chromatography–tandem mass spectrometry (Wallenberg Laboratory at Sahlgrenska University Hospital, Sweden). Plasma AST and ALT levels were measured in the clinical laboratories of the Institute of Clinical Chemistry and Pathobiochemistry in Uniklinik RWTH Aachen. Western blot, real-time PCR, immunostaining, histological analysis, flow cytometry analysis of intrahepatic immune cells, microbiota data analysis and RNA-Seq data analysis are described in detail in the supplementary information. The primers used in the real-time PCR were listed in Supplementary Table S1.

2.3 | Statistics

Statistical analysis was performed in GraphPad Prism 9. Unpaired two-tailed Student's *t*-test was employed for comparisons of two groups. Two-way ANOVA and Tukey's multi-comparisons test was used in grouped diagrams. Data were considered significant between experimental groups as: $^{*}p<0.05$, $^{**}p<0.01$, $^{***}p<0.001$, $^{****}p<0.0001$. Analysis procedure for microbiome and RNA-Seq can be found in the supplementary information.

3 | RESULTS

3.1 | Long term hypercaloric diet exacerbates features of NAFLD in *Pnpla3*$^{148M/M}$ mice

To study the influence of the PNPLA3 I148M genotype on NALFD disease progression *Pnpla3*$^{148M/M}$ knock-in mice, in which hypercaloric feeding is known to cause the enrichment of PNPLA3 on the membrane of lipid droplets,[15] were fed with HFD for 24 and 52 weeks.

When compared to *Pnpla3*^{WT} mice of the same genetic background, *Pnpla3*$^{148M/M}$ animals gained significantly more body weight over time, which was first evident after 17 weeks of HFD (Figure 1A). The highest amount of weight gain was accounted for liver weight (Figure 1B) and subcutaneous adipose tissue mass, according to body composition study upon sacrifice after 52 weeks HFD (Figure 1C). When compared to WT controls, *Pnpla3*$^{148M/M}$ livers were substantially heavier and macroscopically showed steatosis after 52 weeks (Figure 1D). Liver histology revealed abundant hepatic lipid deposition. After 24 weeks HFD, the pattern of ballooning degeneration was comparable between both genotypes. However, *Pnpla3*$^{148M/M}$ livers showed more parenchymal and non-parenchymal cells including immune cells at 52 weeks (Figures 1E and S1A). In *Pnpla3*$^{148M/M}$ mice, serum liver injury markers (AST, ALT) were significantly higher compared to *Pnpla3*^{WT} mice after 24 and 52 weeks (Figure 1F,G). With a selected range of body weight, *Pnpla3*$^{148M/M}$ mice have higher mean AST values compared to WT mice but did not reach statistically significant differences after 16 and 24 weeks of HFD (Figure S3F). *Pnpla3*$^{148M/M}$ mice fed with HFD showed significantly more liver lipids than WT mice (Figure 1H,I).

In summary, the data demonstrate that long term HFD feeding resulted in a significantly more pronounced NASH-related phenotype in *Pnpla3*$^{148M/M}$ compared to *Pnpla3*^{WT} mice.

3.2 | HFD triggers a stronger inflammatory response in *Pnpla3*$^{148M/M}$ livers

Inflammation is a driver of liver injury and consecutively triggers fibrosis progression. As a result, we investigated the presence of relevant immune cell populations in the liver tissue of our animals. In comparison to *Pnpla3*^{WT} controls, *Pnpla3*$^{148M/M}$ mice had more CD45^{+} inflammatory cells in their livers after HFD feeding for 52 weeks. In contrast, no significant differences were found after 24 weeks of HFD (Figure 2A,B). Thus, we concentrated on the 52 weeks timepoint for more detailed analysis. Flow cytometry of immune cells from liver tissue showed increased numbers of CD45^{+} cells in *Pnpla3*$^{148M/M}$ mice (Figure 2C). After 52 weeks, HFD *Pnpla3*$^{148M/M}$ livers compared to *Pnpla3*^{WT} controls had more CD8^{+} and NK T-lymphocytes and NK cells among those cells (Figure 2D–F). Furthermore, monocyte-derived macrophages were significantly higher in *Pnpla3*$^{148M/M}$ compared to WT livers (Figure 2G). CD11b^{+} Ly6G^{+} neutrophils were increased, in line with these findings (Figure 2H). The PNPLA3 I148M mutation triggers STAT3 activation both in vivo and in vitro.[17,18] Western Blot analysis revealed that P-STAT3 expression was increased only after 52 weeks of HFD feeding in *Pnpla3*$^{148M/M}$ livers compared to *Pnpla3*^{WT} livers (Figure 2I). Livers of NEMO$^{\Delta hepa}$/JNK$^{\Delta hepa}$ mice[19] were used as a positive control.

Hence, these results showed that HFD in *Pnpla3*$^{148M/M}$ livers leads to a stronger inflammatory response compared to WT controls.

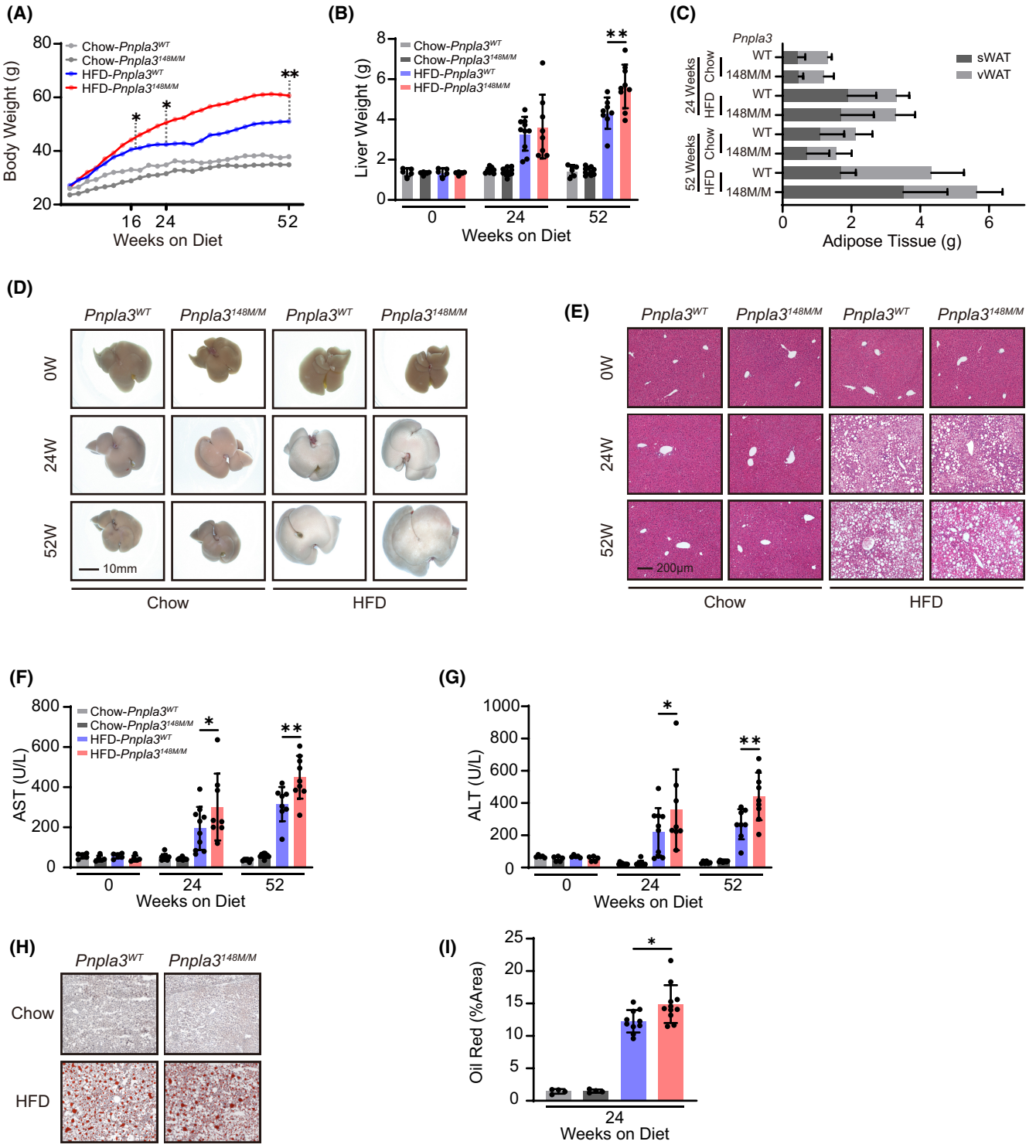

3.3 | Distinct proliferative pattern in *Pnpla3*$^{148M/M}$ livers after long term hypercaloric diet

Increased liver cell proliferation is characteristic of NAFLD and is required for the initiation and progression of hepatic fibrosis in both human and animal models of the disease.[20,21] Since *Pnpla3*$^{148M/M}$ livers had increased cell numbers per view field in H&E staining after 52 weeks HFD feeding, we stained liver tissue for Ki-67 to study changes in hepatic cell proliferation. In the livers of *Pnpla3*$^{148M/M}$ mice, we found a significant increase in Ki-67 positive cells after 24 and 52 weeks of HFD (Figure 3A,B). In line with increased proliferation, Tunel staining of liver tissue suggested increased cell death after HFD. Tunel positivity was significantly higher in *Pnpla3*$^{148M/M}$ compared to WT livers after 24 and 52 weeks of HFD feeding (Figures 3C and S1B). Further analysis showed higher staining for cleaved caspase 3 in *Pnpla3*$^{148M/M}$ livers under HFD after 52 weeks

FIGURE 1 Long term hypercaloric diet exacerbates features of NAFLD in *Pnpla3*$^{148M/M}$ mice. (A) *Pnpla3*^{WT} and *Pnpla3*$^{148M/M}$ mice were treated with diet experiments at around 8–10 weeks old and were fed with HFD or chow diet for up to 52 weeks. *Pnpla3*$^{148M/M}$ mice receiving HFD showed significant differences in body weight from 17 weeks. Each value represents the mean value of one group and shown as every 2 weeks. Two-way ANOVA and Tukey's multiple comparisons test were performed. ($n = 5$–10/group) $^{*}p \leq 0.05$, $^{**}p \leq 0.01$. (B) The liver weight is shown before feeding (0 weeks) and after 24 and 52 weeks of feeding. *Pnpla3*$^{148M/M}$ mice fed with HFD had more liver weight at 52 weeks. Data is represented as mean ± SD. Two-way ANOVA and Tukey's multiple comparisons test were performed. $^{*}p \leq 0.05$, $^{**}p \leq 0.01$ ($n = 5$–10/group). (C) Adipose tissue weight from both PNPLA3 genotypes fed with chow diet and HFD for 24 and 52 weeks. *Pnpla3*$^{148M/M}$ mice with HFD gained more weight of sWAT at 52 weeks. ($p \leq 0.0001$) Values are presented as mean ± SD. Two-way ANOVA and Tukey's multiple comparisons test were performed. ($n = 5$–10/group). (D) Macroscopic pictures of liver of each genotype are shown for 0, 24, 52 weeks of feeding. (E) Representative H&E staining (10X) before feeding and at 24 and 52 weeks of treatment. (F, G) Serum levels of ALT (F) and AST (G) measured upon sacrifice after 0, 24 and 52 weeks of feeding. The liver transaminases were higher in *Pnpla3*$^{148M/M}$ mice at 24 and 52 weeks. Data are represented as mean ± SD. Two-way ANOVA and Tukey's multiple comparisons test were performed. ($n = 5$–10/group) $^{*}p \leq 0.05$, $^{**}p \leq 0.01$. (H) Representative Oil Red O staining for mice from both genotypes at 24 weeks' time point. (I) Quantification of Oil Red staining. Data are represented as mean ± SD. Two-way ANOVA and Tukey's multiple comparisons test were performed. ($n = 4$–10/group) $^{*}p \leq 0.05$. ALT, alanine transaminase; AST, aspartate transaminase; HFD, high fat diet; sWAT, subcutaneous white adipose tissue; vWAT, visceral adipose tissue.

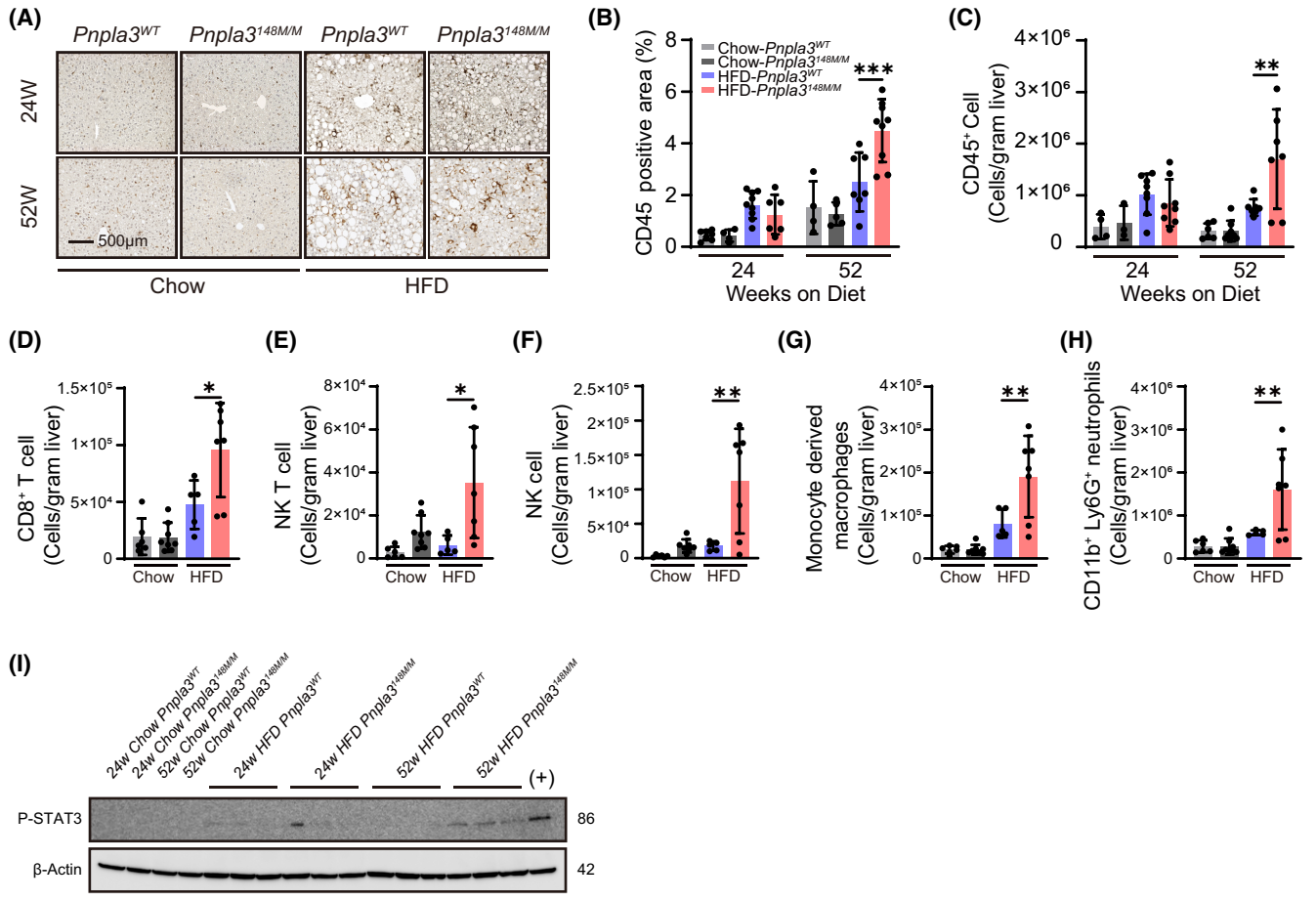

FIGURE 2 HFD triggers a stronger inflammatory response in *Pnpla3*$^{148M/M}$ livers. (A) Representative CD45^{+} staining (10X) images of liver tissue from *Pnpla3*^{WT} and *Pnpla3*$^{148M/M}$ animals fed with chow diet or HFD for 24 and 52 weeks ($n = 4$–9/group). (B) Quantification of CD45^{+} staining by the percentage area of positive cells per view field. More CD45^{+} immune cells infiltrated in *Pnpla3*$^{148M/M}$ mice liver at 52 weeks. Data are shown as mean ± SD. Two-way ANOVA and Tukey's multiple comparisons test were performed. ($n = 4$–9/group) $^{***}p \leq 0.001$. (C) CD45^{+} quantification of liver immune cells by FACS analysis after 24 and 52 weeks of feeding using both genotypes. Data showed that the *Pnpla3*$^{148M/M}$ mice liver had more CD45^{+} immune cells infiltrated after 52 weeks HFD feeding. Data are shown as mean ± SD. Two-way ANOVA and Tukey's multiple comparisons test were performed. ($n = 4$–8/group). $^{**}p \leq 0.01$. (D–H) Different immune cell liver subsets were isolated from mice liver and quantified by FACS analysis in both genotypes after 52 weeks of chow or HFD feeding. CD8^{+} T cells (D), NK T cells (E), NK cells (F), monocytes derived macrophages (G) and CD11b Ly6G neutrophils (H) are significantly increased upon HFD in the I148M group. ($n = 5$–8/group). Data are shown as mean ± SD. Two-way ANOVA and Tukey's multiple comparisons test were performed. $^{*}p \leq 0.05$, $^{**}p \leq 0.01$. (I) Representative Western Blot for P-STAT3 from mouse livers after 24 and 52 weeks of feeding showing both genotypes. (+) refers to positive control.

(Figure 3D,E). Stronger cell proliferation in NASH can potentially be explained by a stronger ductular response.[22] Here we found increased cytokeratin-19 (CK19) positive cells after 24 and 52 weeks HFD in *Pnpla3*$^{148M/M}$ compared to *Pnpla3*^{WT} livers (Figure 3F,G). When the animals were separated by body weight, we found that CK19 positive area in the livers was linked to increased body weight in *Pnpla3*$^{148M/M}$ mice, but not in WT mice fed an HFD for 52 weeks (Figure 3H). However, it should be considered that on average *Pnpla3*$^{148M/M}$ mice gained more weight under HFD than WT animals.

We next investigated whether enhanced ductular proliferation influences bile acids (BAs) levels in the liver and faeces. After 52 weeks of HFD, there were no differences in hepatic Bas levels between WT and *Pnpla3*$^{148M/M}$ mice (Figure 3I). However, rectal faeces samples from *Pnpla3*$^{148M/M}$ mice exhibited considerably higher BAs levels after 52 weeks (Figure 3J). Additionally, HFD induced significantly higher cholesterol levels and *CYP7A1* expression than chow diet mice after 52 weeks (Figure 3K,L). Besides, *NTCP* was downregulated after HFD feeding (Figure 3M).

Thus, in comparison to WT mice, cell proliferation and cell death were major discriminating factors of the phenotype of NAFLD in *Pnpla3*$^{148M/M}$ livers, and faecal BAs were increased most likely as a result of dysregulated bile acid metabolism.

3.4 | Susceptibility to liver fibrosis is increased in *Pnpla3*$^{148M/M}$ mice after long term hypercaloric diet

In humans, the PNPLA3 I148M polymorphism has been linked to more severe liver fibrosis.[2] Here we studied the impact of the PNPLA3 I148M genotype on fibrosis in a long term HFD mouse model.

HFD feeding increased hepatic fibrosis detected by Sirius Red staining (Figure 4A) in both genotypes after 52 weeks. Importantly, fibrosis progression was significantly more pronounced in *Pnpla3*$^{148M/M}$ livers compared to controls after quantification of the Sirius Red positive area (Figure 4B). Next, proteins linked to liver fibrosis and hepatic stellate cell activation were investigated. After 52 weeks of HFD, desmin expression was elevated in *Pnpla3*$^{148M/M}$ compared to *Pnpla3*^{WT} control livers (Figure 4C,D). Representative Western Blot analysis for alpha SMA of entire liver lysates from 52 weeks fed animals further strengthened these findings (Figure 4E,F). Since PNPLA3 protein expression was associated with HSCs activation, we analysed PNPLA3 protein expression. There was a trend that *Pnpla3*$^{148M/M}$ mouse livers expressed more PNPLA3 protein compared to *Pnpla3*^{WT} mice after 52 weeks HFD. However, these differences did not reach statistical significance (Figure S3G,H). As we fasted the animals for 3 h before sacrificing, and PNPLA3 protein expression is regulated via food intake,[23] this might influence PNPLA3 protein expression.

In conclusion, HFD triggered a more pronounced fibrotic reaction in *Pnpla3*$^{148M/M}$ compared to *Pnpla3*^{WT} control animals.

3.5 | Exacerbated NAFLD in *Pnpla3*$^{148M/M}$ mice show a distinct intestinal microbial pattern, associated with obesity and high fat diet

The intestine microbiome is becoming increasingly recognized as a driver in various diseases, and changes have been connected to disease progression in obesity and NAFLD.[24] To explore the effect of host genotype on microbiome composition, faecal samples collected from *Pnpla3*^{WT} and *Pnpla3*$^{148M/M}$ mice fed on chow and HFD for 52 weeks were subjected to 16S rRNA gene sequencing. The microbial composition was compared between the genetic groups on a single diet and in between diet groups for an individual genotype. There was no difference observed in alpha diversity in terms of Shannon Index and Chao1 between the genotypic groups on either of the diets (Figure 5A). However, *Pnpla3*$^{148M/M}$ mice showed a significantly increased representation of Firmicutes members, while Bacteroidetes were decreased following HFD feeding

FIGURE 3 Distinct proliferative pattern in *Pnpla3*$^{148M/M}$ livers after long term hypercaloric diet. (A) Quantification of Ki-67 staining positive cells per view field. *Pnpla3*$^{148M/M}$ mice fed with HFD showed more proliferation in the liver at both 24 and 52 weeks. ($n = 5$–6/group) $^{*}p \le 0.05$, $^{***}p \le 0.001$ (B) Representative images of Ki-67 staining of liver slides in both genotypes upon 24 and 52 weeks of feeding. (C) Quantification of Tunel positive cells per field view from both genotypes after 24 and 52 weeks time point. Data indicate that there was more cell death in *Pnpla3*$^{148M/M}$ mice fed with HFD at 24 and 52 weeks. $^{**}p \le 0.01$, $^{***}p \le 0.001$ ($n = 4$–10/group). (D) Representative images of cleaved caspase 3 immunofluorescence staining in the respective livers are shown after 24 and 52 weeks of feeding. (E) Quantification of cleaved caspase 3 staining. Percentage of positive cells to the total number of DAPI positive nuclei per view field from both genotypes after 24 and 52 weeks time point. The expression of cleaved caspase 3 was upregulated in *Pnpla3*$^{148M/M}$ mice fed with HFD at 52 weeks. ($n = 4$–6/group) $^{**}p \le 0.01$ (F) Quantification of CK-19 positive area per view field. More CK19 positive cells were observed in *Pnpla3*$^{148M/M}$ mice at 24 and 52 weeks in HFD. ($n = 4$–10/group). $^{**}p \le 0.01$ (G) Liver CK19 IHC staining (10X) at the time points 24 and 52 weeks after feeding. (H) Linear regression analysis of CK19 positive area per view field versus body weight in *Pnpla3*^{WT} and *Pnpla3*$^{148M/M}$ HFD group at 52 weeks. (I, J) Total bile acids in the liver (I) and from rectal faeces (J) were measured in samples of mice fed for 24 and 52 weeks with chow and HFD. Rectal faeces sample from *Pnpla3*$^{148M/M}$ mice fed with HFD contained more total bile acids at 52 weeks. ($n = 4$–6/group) $^{*}p \le 0.05$. (K) Serum cholesterol level from mice fed with chow or HFD for 52 weeks in both genotype. Mice with HFD have significantly higher cholesterol level than chow diet mice. ($n = 6$–12/group) $^{****}p \le 0.0001$. (L, M) Real-time PCR analysis of *CYP7A1* (L) *and NTCP* (M) in *Pnpla3*$^{148M/M}$ and *Pnpla3*^{WT} livers after 52 weeks of feeding. Normalized to the *Pnpla3*^{WT} chow diet group, mice with HFD showed higher *CYP7A1* expression and lower *NTCP* expression levels. ($n = 5$–6/group) $^{*}p \le 0.05$, $^{****}p \le 0.0001$ In (B, D, G–M) data are shown as mean ± SD. Two-way ANOVA and Tukey's multiple comparisons test were performed. CC-3, cleaved caspase 3; BAs, bile acids; CYP7A1, cytochrome P450 family 7 subfamily A member 1; NTCP, sodium taurocholate co-transporting polypeptide.

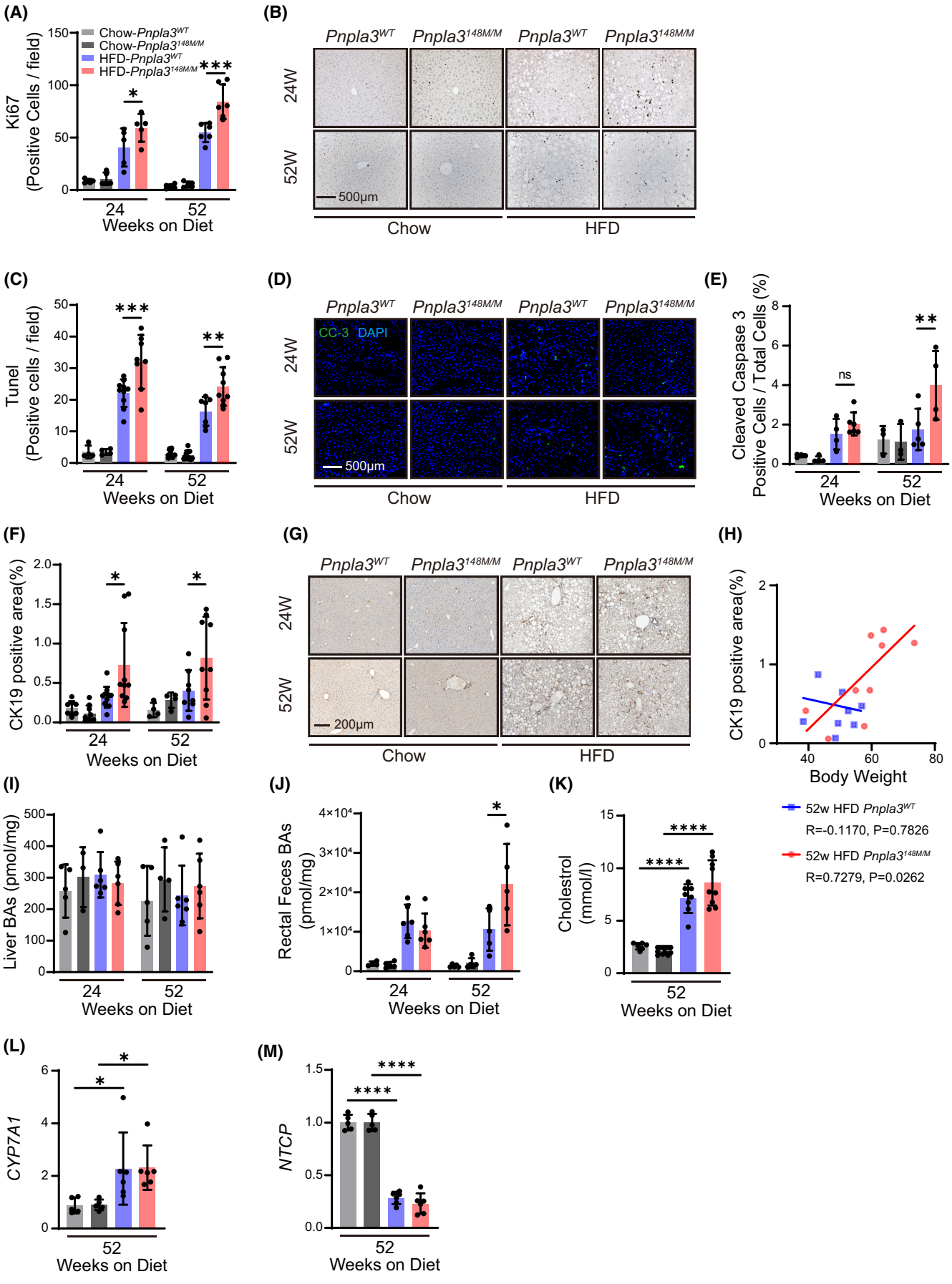

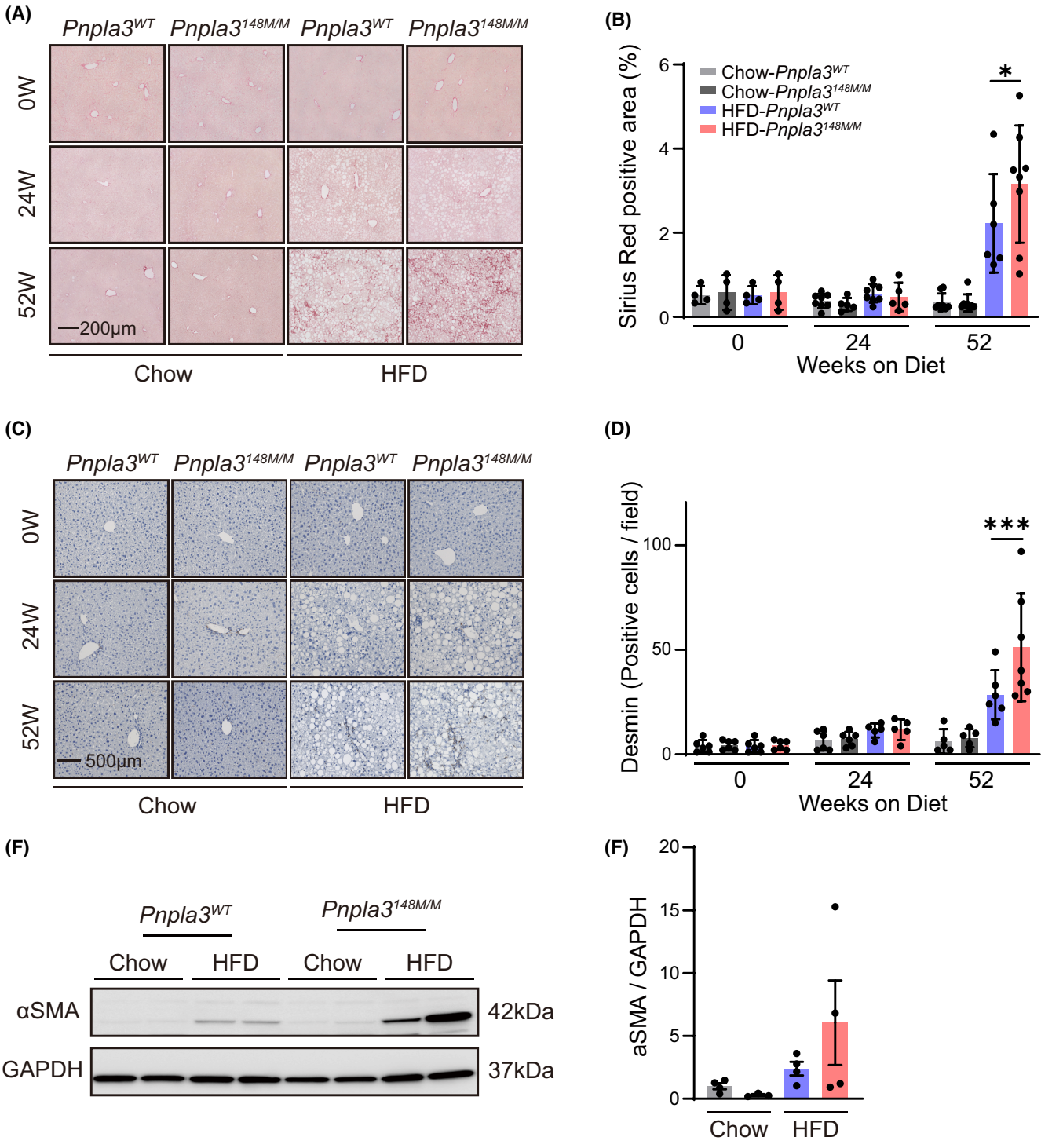

FIGURE 4 Susceptibility to liver fibrosis is increased in *Pnpla3*$^{148M/M}$ mice after long term HFD. (A) Representative images of Sirius red staining from liver slides of each genotype fed for 0, 24 and 52 weeks. (B) Quantification of Sirius red staining depicting the percentage of fibrotic areas per view field. Data indicating that liver fibrosis is increased in *Pnpla3*$^{148M/M}$ mice fed with HFD at late time point. Data are shown as mean ± SD. Two-way ANOVA and Tukey's multiple comparisons test were performed. ($n = 4–8$/group). *$p \leq 0.05$. (C) Representative images of desmin staining from liver slides of each genotype fed for 0, 24 and 52 weeks. (D) Quantification of desmin positive cells per view field. The number of cells expressing desmin were higher in *Pnpla3*$^{148M/M}$ mice fed with HFD at 52 weeks. Data are shown as mean ± SD. Two-way ANOVA and Tukey's multiple comparisons test were performed. ($n = 5–8$/group) ***$p \leq 0.001$. (E) Western Blot analysis for liver α-SMA was performed at 52 weeks of feeding as indicated. (F) Quantification of α-SMA Western Blot analysis from an independent experiment in both genotypes after 52 weeks of chow or HFD feeding. Two-way ANOVA and Tukey's multiple comparisons test were performed. Data are shown as mean ± SD.

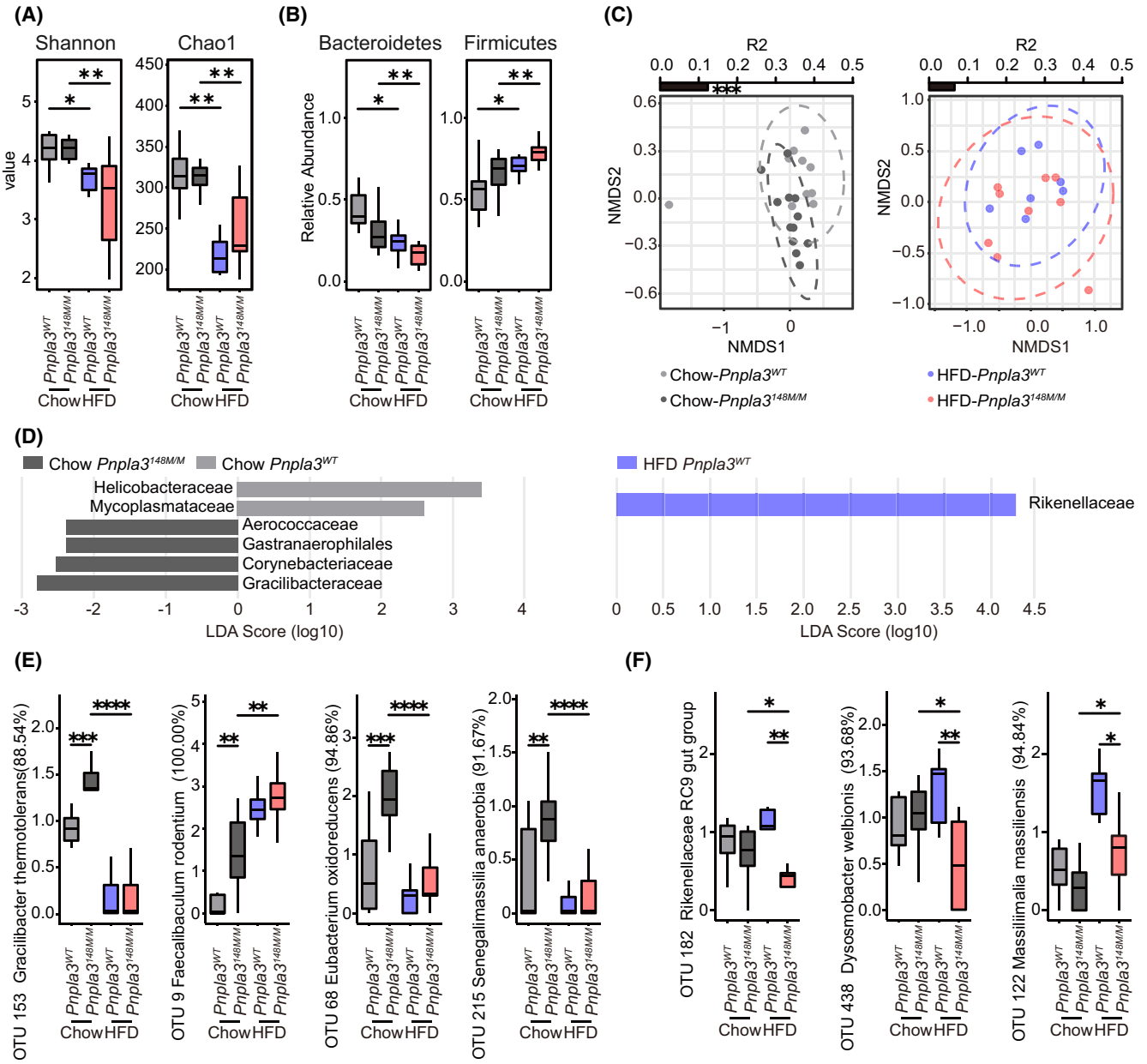

FIGURE 5 Exacerbated NAFLD in *Pnpla3*$^{148M/M}$ mice show a distinct intestinal microbial pattern, associated with obesity and western diet. All microbiota results are reported from the 52 weeks timepoint. In *Pnpla3*^{WT} chow group, $n=10$, in *Pnpla3*$^{148M/M}$ chow group, $n=12$, in *Pnpla3*^{WT} HFD group, $n=7$, in *Pnpla3*$^{148M/M}$ HFD group, $n=9$. (A) Alpha diversity in terms of Shannon Index and Chao1 in between the genotypic groups on either of the diet. Alpha diversity difference could only be observed between diet in each genotype. Data was shown as mean ± SD. $^{*}p \le 0.05$, $^{**}p \le 0.01$. (B) Relative abundance of *Firmicutes* and *Bacteroidetes* in chow diet and HFD in 52 weeks. The relative abundance of *Firmicutes* and *Bacteroidetes* reached significant differences after HFD feeding in each genotypic group. Data was shown as mean ± SD. $^{*}p \le 0.05$, $^{**}p \le 0.01$. (C) NMDS on chow and HFD and individual effect size of the diet groups using pairwise comparison. Gut microbiota composition showed difference in chow diet between the groups. The samples clustered within 95% confidence ellipse within respective groups. (D) Linear discriminant analysis (LDA) of taxonomic biomarkers at the family level in chow diet or HFD. (E, F) Relative abundance of DA OTUs for the relevant groups. Data was shown as mean ± SD. $^{*}p \le 0.05$, $^{**}p \le 0.01$, $^{***}p \le 0.001$, $^{****}p \le 0.0001$. DA, differential abundance; OTU, operative taxonomic unit.

(Figure 5B). *Pnpla3*^{WT} and *Pnpla3*$^{148M/M}$ mice fed a HFD did not show any difference in gut microbiota composition ($R^2=0.06591$, $Pr(>F)=0.403$), while mice on chow diet showed difference between the groups ($R^2=0.12368$, $Pr(>F)=0.001$) (Figure 5C). On the contrary, both *Pnpla3*^{WT} and *Pnpla3*$^{148M/M}$ mice showed an expected difference in microbiota composition in terms of both alpha and beta diversity when compared between chow and HFD (Figures 5A and S1C).

Linear discriminant analysis (LDA) was performed to identify taxonomic biomarkers at the family level and OTUs (Operational Taxonomic Units) were picked out for the relevant groups using the negative binomial Wald test. *Pnpla3*$^{148M/M}$ mice on chow diet

showed enriched *Gracilibacteraceae* (Figure 5D) and from this family *Gracilibacter thermotolerans* (OTU 153) was significantly enriched ($p=0.007$) compared to that of *Pnpla3*^{WT} mice. Besides, *Faecalibaculum rodentium* (OTU 9), *Eubacterium oxidoreducens* (OTU 68) and *Senegalimassilia anaerobia* (OTU 215) were other species that were significantly enriched in *Pnpla3*$^{148M/M}$ mice (Figures 5E and S1D). Following HFD, *Faecalibaculum rodentium* (OTU 9) was further enriched in *Pnpla3*$^{148M/M}$ mice. *Rikenellaceae RC9 gut group* (OTU 182) from the family *Rikenellaceae* was significantly less abundant ($p=0.0041$) in *Pnpla3*$^{148M/M}$ mice on HFD (Figures 5D,F and S1D). *Dysosmobacter welbionis* (OTU 438) and *Massiliimalia massiliensis* (OUT 122) were two other species that were less abundant in *Pnpla3*$^{148M/M}$ mice following HFD feeding when compared to that of *Pnpla3*^{WT} mice (Figures 5F and S1D). In addition, in the comparison of diet in each genetic group, the families *Erysipelotrichaceae*, *Enterobacteriaceae*, *Deferribacteraceae* and *Coriobacteriaceae* were altered (Figure S1E).

Taken together, HFD diet induced faecal microbial composition and diversity alteration which contributed to around 36% of total variation, while the genotype (*Pnpla3*$^{148M/M}$ versus WT) under HFD contributed 12% of the variation.

3.6 | Transcriptional analysis revealed genes involved in NAFLD progression and specific genes altered by PNPLA3 I148M

To compare HFD-induced expression changes in *Pnpla3*^{WT} and *Pnpla3*$^{148M/M}$ livers, RNA-Seq analyses were performed after 24 weeks of high fat or chow diet. The time point of 24 weeks was chosen to study early events, since HFD did not yet induce fibrosis after this exposure time (Figure 3A,B), whereas liver enzymes (Figure 1E,F) were already increased. Principle component analysis demonstrated that *Pnpla3*^{WT} and *Pnpla3*$^{148M/M}$ mice were clearly separated along PC2 (Figure 6A). Moreover, HFD had a strong influence and caused a shift from right to left along PC1. While the mice under the chow diet clustered relatively closely together, animals under HFD showed a larger variability along PC1.

Next, differentially expressed genes were visualized by volcano plots (Figure 6B–E; Tables S2–S9). HFD induced strong gene expression changes in both *Pnpla3*^{WT} (Figure 6B) and *Pnpla3*$^{148M/M}$ (Figure 6C) livers. The number of upregulated genes was approximately twice as high as the number of downregulated genes. Compared to the influence of HFD, the number of differential genes between *Pnpla3*^{WT} and *Pnpla3*$^{148M/M}$ in either the HFD (Figure 6D) or the chow diet group (Figure 6E) was much lower. Overrepresentation analysis of the differential genes in Figure 6B–E demonstrated that genes upregulated due to HFD were overrepresented in inflammation and immune response associated GO terms (Figure S2A–D). In contrast, the downregulated genes were dominated by metabolic processes, such as cholesterol and steroid biosynthetic processes and further differentiated liver functions (Figure S2E–H). Overrepresentation analysis of genes differentially expressed between *Pnpla3*^{WT} and *Pnpla3*$^{148M/M}$ did not result in significant GO terms after adjustment for multiple testing.

To identify possible differences in global gene expression changes between mutant and wild-type mice, the fold-changes of individual genes between chow and HFD were plotted for *Pnpla3*^{WT} and *Pnpla3*$^{148M/M}$ mice (Figure 6F). The scatter plot of individual genes showed a strong correlation of HFD-induced expression changes in both mouse strains. Validated with qPCR, we found a similar strong induction by HFD for example for *Ccr1*, *Ccr5* and *Ccr2*, genes that may trigger an inflammatory response (Figure S3A–C) and for *Timp1* and *Vcan* that are involved in fibrogenesis (Figure S3D,E), corresponding to the NAFLD phenotypes in humans.[25,26] However, for several genes the $\log_2$-fold change differed by more than 0.5 in WT and mutant mice. The dots for these genes appeared outside the blue lines in Figure 6F. For a set of 171 genes, indicated as 'group 1' in Figure 6F, HFD caused a stronger increase in *Pnpla3*$^{148M/M}$ than in *Pnpla3*^{WT} livers (list of genes in Tables S10 and S11). These genes were overrepresented predominantly in immune associated GO groups (Figure 6G). Among the genes more upregulated in the livers of mutant than WT mice after 52 weeks of HFD were *Cracc* and *Eat2* (Figure 7A,B). It was reported that CRACC can inhibit NK- and T-cell function in the absence of EAT2. However, with the participation of EAT2, CRACC can positively regulate NK cells and T cells, which promotes inflammation.[27] *Ephb2* expressed in HSCs is a crucial gene that regulates *Ccl2* and *Ccr2* expression.[28,29] *Ephb2* was significantly increased in *Pnpla3*$^{148M/M}$ livers both at 24 and 52 weeks (Figure 7C). Osteopontin encoded by *Spp1* and expressed in macrophages, is a biomarker for liver damage and fibrosis.[30] Here we found that *Spp1* expression was higher in *Pnpla3*$^{148M/M}$ mice at 52 weeks (Figure 7D). Besides, *Pilrα*, which reduces macrophage infiltration,[31] was dramatically decreased in *Pnpla3*$^{148M/M}$ livers (Figure 7E). To confirm our finding, Clec4f staining was performed. Kupffer cells were significantly enriched in *Pnpla3*$^{148M/M}$ livers at 52 weeks (Figure 7F,G). The proinflammatory chemokine *Ccl2* was increased in line with this finding (Figure 7H). Osteopontin staining confirmed mRNA analysis (Figure 7J,K).

Taken together, the PNPLA3 I148M genotype was associated with genes involved in inflammation and fibrogenesis and may contribute to stronger NAFLD-dependent disease progression.

4 | DISCUSSION

In the present study, we used a knock-in mouse model for PNPLA3 to mimic the most common genetic risk factor for disease progression of metabolic liver injury the PNPLA3 I148M genotype. This model helps to better understand findings in humans,[32] but also adds essential knowledge to previous findings in the PNPLA3 mouse model.[15] In animals with the I148M substitution we found increased liver damage, fibrosis, alterations in intestinal microbiota and a cluster of genes associated with stronger HFD-induced expression in PNPLA3 I148M compared with WT mice. These observations were only found after long term HFD feeding.

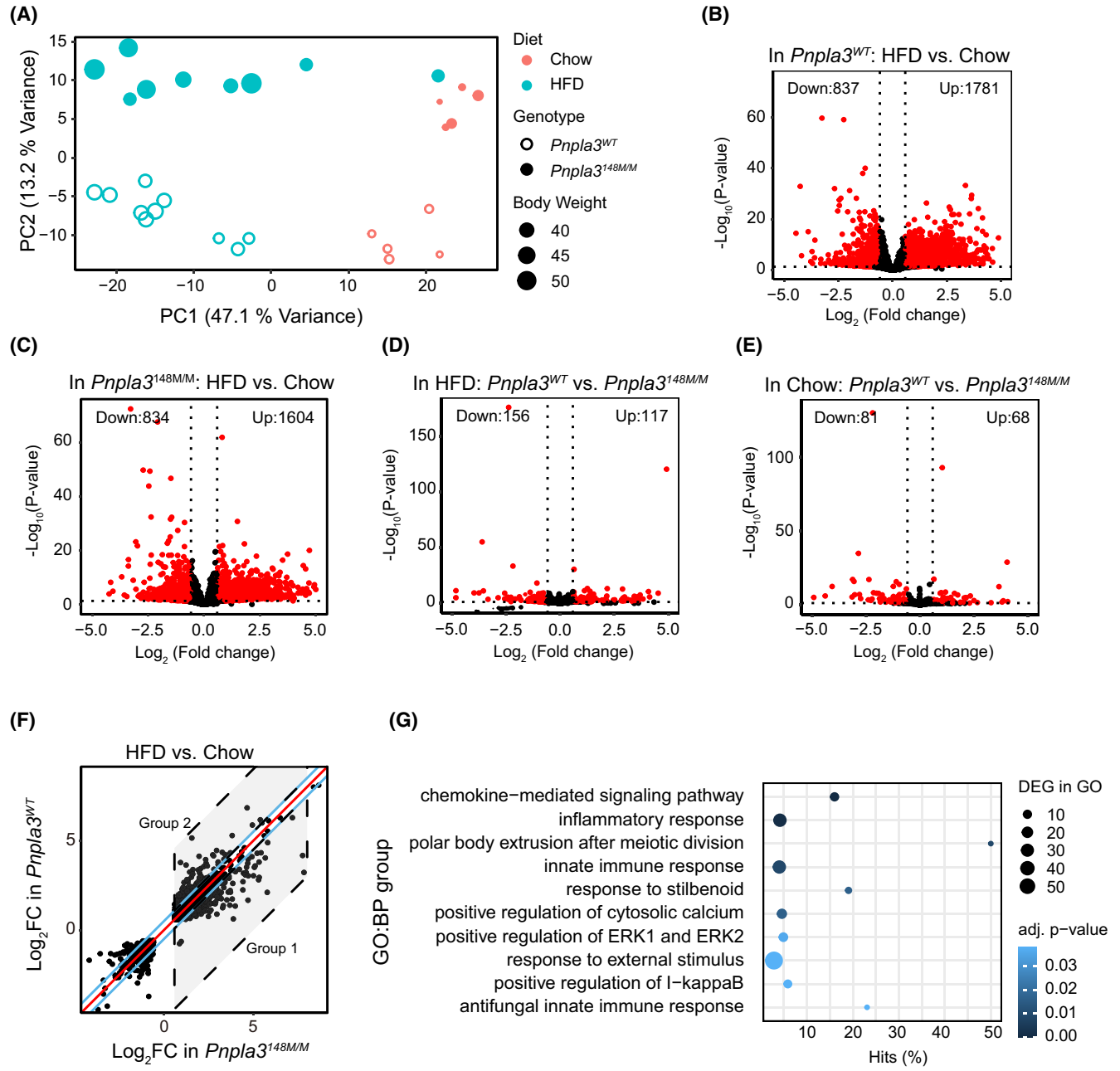

FIGURE 6 HFD induced gene expression alterations in *Pnpla3*$^{148M/M}$ and *Pnpla3*^{WT} mice. (A) Principal component analysis of the *Pnpla3*^{WT} and *Pnpla3*$^{148M/M}$ mice. Red and blue differentiates chow and HFD, respectively. The size of the symbols represents the body weight of the individual mice. (B–E) Volcano plot representation of the differential genes between *Pnpla3*^{WT} HFD and chow group (B), *Pnpla3*$^{148M/M}$ HFD and chow group (C), *Pnpla3*^{WT} HFD and *Pnpla3*$^{148M/M}$ HFD group (D), *Pnpla3*^{WT} chow and *Pnpla3*$^{148M/M}$ chow group (E). (F) Scatter plot of the fold-changes induced by HFD for individual genes for *Pnpla3*$^{148M/M}$ and *Pnpla3*^{WT}mice. Only genes with a fold change of at least $\sqrt{2} = 1.41$ (difference of 0.5 on log2-scale) and an fdr-adjusted *p*-value < 0.05 are shown. The red line is the diagonal line; blue lines indicate a 4-fold difference of 2 to the diagonal line (log2-scale). The dotted scores indicate genes with at least 1.41-fold higher (group 1) or lower (group 2) fold-changes in *Pnpla3*$^{148M/M}$ compared to *Pnpla3*^{WT} mice. (G) GSEA analysis of DEGs in group 1 of Figure 6F. The *p*-values of the GO groups of the BP are adjusted with an FDA of 0.05 and colour coded. A darker colour indicates a smaller adjusted p value. Hits [%] on the x axis is the proportion of group 1 genes in the respective GO group. The size of the circles indicated the size or total number of genes in the respective GO group. DEGs, differentially expressed genes; GO, gene ontology; BP, biological processes; FDA, false discovery rate.

Changes in intestinal microbiota composition has been found in different human cohorts with liver diseases including NASH. These findings reflect a dysregulation within the gut-liver axis and earlier results including our own recent data suggest that this finding is associated with increased bacterial translocation triggering a stronger inflammatory milieu in the liver.[24] In our study, we saw a decrease in microbial diversity under HFD consistent with prior findings. These effects were mainly diet-dependent rather than

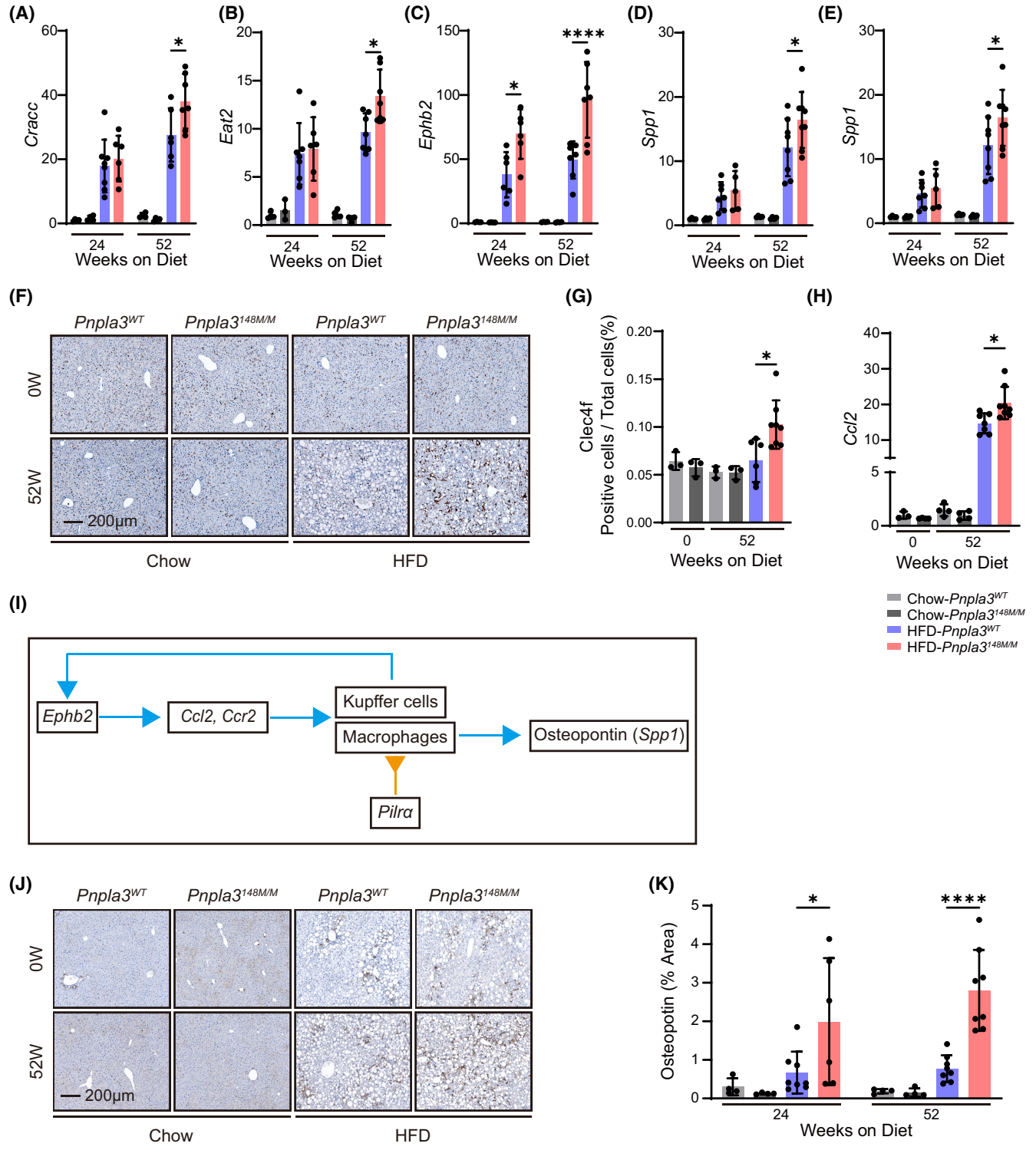

genotype-dependent, highlighting the relevance of nutrition in microbial gut composition.[33] *Ruminococcaceae* were previously shown to be enriched in HFD while *Provotellaceae* and *Bacteroidales* S24-7 groups which are now known as *Muribaculaceae* were decreased and this pattern complied with our models.[34,35] *Bacteroidaceae* was more abundant after 52 weeks HFD in both genotypes.

When the effect of the genotypes *Pnpla3*$^{148M/M}$ versus the *Pnpla3*^{WT} group after HFD feeding was compared, significant alterations were observed at the OTU level. The *Rikenellaceae RC9 gut group* (OTU 182) belonging to the *Rikenellaceae* family, *Dysosmobacter welbionis* (OTU 438) and *Massiliimalia massiliensis* (OUT 122) from the *Ruminococcaceae* family was significantly reduced in the *Pnpla3*$^{148M/M}$ group on HFD, while the relative abundance on chow diet in both genotypes did not show significant differences. There was also a compositional difference observed between the genotypes on chow diet. *Faecalibaculum rodentium* (OTU

FIGURE 7 Specific genes altered by *Pnpla3*$^{148M/M}$ and the relation to macrophages and Kupffer cells. (A–E) Real-time PCR analysis of *Cracc* (A), *Eat2* (B), *Ephb2* (C), *Spp1* (D), and *Pilrα* (E) based on list from group 1 and group 2 in Figure 6F with different expression induced by HFD in *Pnpla3*$^{148M/M}$ and *Pnpla3*^{WT} mice. Normalized to the time point 24 weeks in *Pnpla3*^{WT} chow diet mice. Data are shown as mean ± SD. Two-way ANOVA and Tukey's multiple comparisons test were performed. ($n = 4–8$/group) $^{*}p \le 0.05$, $^{**}p \le 0.01$, $^{****}p \le 0.0001$. (F) Representative images (10X) of Clec4f IHC staining from both genotypic groups at 0 and 52 weeks. (G) Analysis of Clec4f staining by the percentage of positive cells to the total number of cells per view field from both genotypes at before feeding (0) and after 52 weeks. More clec4f positive cells infiltrated in *Pnpla3*$^{148M/M}$ mice fed with HFD at 52 weeks. Data are shown as mean ± SD. ($n = 3–8$/group) Two-way ANOVA and Tukey's multiple comparisons test were performed. $^{*}p \le 0.05$. (H) Real-time PCR analysis of *Ccl2* gene expression from mice fed in 0 or 52 weeks timepoint. Ccl2 expression level was higher in *Pnpla3*$^{148M/M}$ mice liver fed with HFD. Normalized by 0 weeks Chow diet fed *Pnpla3*^{WT} mice. Two-way ANOVA and Tukey's multiple comparisons test were performed. ($n = 3–8$/group) $^{*}p \le 0.05$. (I) Diagram about how the *Ephb2*, *Ccl2*, *Ccr2*, *Pilrα* influence macrophages, Kupffer cells and Osteopontin. *Ephb2* is essential for the expression of *Ccl2* and *Ccr2*. *Ccl2* and *Ccr2* are involved in the recruitment of macrophages to the liver. Besides, Kupffer cells are the key regulator of *Ephb2*. *Pilrα* could decrease the infiltration of macrophages in the liver. Osteopontin expressed by macrophages is a biomarker for fibrosis and liver injury during the progression of NAFLD. (J, K) Representative images (J) and quantification (K) of immunohistochemistry for Osteopontin. Two-way ANOVA and Tukey's multiple comparisons test were performed. Data are shown as mean ± SD. ($n = 4–9$/group) $^{*}p \le 0.05$, $^{****}p \le 0.0001$. Clec4f, C-Type Lectin Domain Family 4 Member F; *Ccl2*, CC-chemokine ligand 2; *Ccr2*, chemokine (C-C motif) receptor 2; *Ephb2*, Eph receptor B2; *Spp1*, secreted phosphoprotein 1; *Pilra*, paired immunoglobin-like type 2 receptor alpha.

9) in *Pnpla3*$^{148M/M}$ mice was significantly more abundant compared to *Pnpla3*^{WT} mice on chow diet and further elevated following feeding with HFD showing a diet dependent pattern, while *Gracilibacter thermotolerans* (OTU 153) had lowered abundance following HFD regardless of genotypes. Together, these findings show that the altered microbiota community confers to 36% to HFD in general and to 12% to the *Pnpla3*$^{148M/M}$ genotype. Changes in microbiota diversity influence liver tissue via translocation of metabolic products, resulting in aggravation of NAFLD. Hence these differences may contribute to changes in liver mRNA expression between the two PNPLA3 genotypes.

Altered BAs concentrations in the gut have been linked to initiation and progression of NAFLD.[36] We found an increase in total bile acids in faeces of *Pnpla3*$^{148M/M}$ compared with mice *Pnpla3*^{WT} mice, supporting prior NAFLD studies.[36] Serum cholesterol levels were increased after 52 weeks HFD in both genotypes. Additionally, the crucial bile acid synthesis enzyme CYP7A1 was upregulated in those liver. In contrast NTCP, allowing efficient reabsorption and recycling of bile acids, was decreased. Hence BAs metabolism in the liver was not different between *Pnpla3*^{WT} and *Pnpla3*$^{148M/M}$ mice after 52 weeks of HFD. As we found a 12% difference in gut microbiota linked to the PNPLA3 I148M genotype, it is likely that these differences are of relevance to explain the differences in faecal BAs concentration.

Increased cell proliferation following liver injury is a key event that drives progression of NAFLD.[21] We observed an increase in proliferation of liver cells at 24 and 48 weeks after HFD feeding in *Pnpla3*$^{148M/M}$ livers. Importantly, this observation was only obvious after at least 24 weeks of HDF feeding. Earlier results in *Pnpla3*$^{148M/M}$ animals were based on shorter feeding experiments and the phenotype of these animals did not completely reflect the findings in humans.[15,37] We investigated the mode of proliferation by studying ductular proliferation, as cholangiocytes are candidates for increased proliferation. At 24 and 52 weeks, we found significantly higher expression of CK19, as a ductular response marker, in *Pnpla3*$^{148M/M}$ livers compared to WT livers. Chronic liver diseases such as cholestasis, NAFLD, and hepatic fibrosis have all been linked to a stronger ductular response.[22]

Importantly, only after around 16 weeks of HFD, the *Pnpla3*$^{148M/M}$ animals showed a significantly stronger weight gain compared to WT control animals. When we chose a specific range of body weight from 40–50 g, the mean AST values in *Pnpla3*$^{148M/M}$ mice was higher compared with WT animals, not reaching statistical significance. Similar findings were made after 24 weeks of HFD. Hence our finding suggest that higher liver injury was only found after long term HFD feeding of *Pnpla3*$^{148M/M}$ animals reflecting the situation in humans where only patients with high BMI and the PNPLA3 I148M genotype suffer from more progressive metabolic liver disease.[12] In accordance with the human situation, we only observed first signs of more progressive liver disease after 24 weeks. However, the impact on fibrosis progression was only evident after 52 weeks of HFD feeding. This cascade of events agrees with aging in humans showing fibrosis progression only after longer periods of 10–15 years in patients with NASH and not NAFLD. Therefore, our data in the *Pnpla3*$^{148M/M}$ mouse model reflect key aspects of metabolic liver disease in humans. Earlier results using these mice were limited as they used shorter feeding intervals not leading to sufficient obesity.[4,38]

In HFD-fed *Pnpla3*$^{148M/M}$ mice, not only liver weight, but especially subcutaneous adipose tissue contributed significantly to increased body weight. Hence in *Pnpla3*$^{148M/M}$ mice compared to WT controls with increased disease progression the liver-fat axis seems to be stronger activated potentially contributing to the overall phenotype in these animals. In our experiments we found weight gain mainly in subcutaneous adipose tissue. There is evidence in humans that visceral adipose tissue significantly contributes to metabolic syndrome-related diseases.[39] However, in a recent study in NAFLD patients, a link between liver function measured by ALT and adipose tissue mass was described, and here both visceral and subcutaneous adipose tissue contributed to the overall phenotype.[40] Therefore, there is presently a certain lack of data to which increased subcutaneous adipose tissue contributes to the overall liver phenotype.

To better define the molecular mechanism leading to more advanced liver disease progression in *Pnpla3*$^{148M/M}$ livers following long term HFD feeding we included RNA seq analysis. Significant expression differences were obtained between HFD and chow fed animals. Upregulated genes were associated with inflammation and changes in the immune response. Downregulated genes were linked with metabolism and other differentiated functions of the mature liver. This response pattern is known from previous studies after animals were challenged with hypercaloric diets rich in fat and calories[16,41] but also for toxic liver injury.[42] As expected, large sets of genes were regulated similarly in response to HFD in *Pnpla3*$^{148M/M}$ and *Pnpla3*^{WT} livers. Interestingly, a specific set of genes associated with immune regulation responded stronger to HFD in *Pnpla3*$^{148M/M}$ compared to wild-type livers.

In the natural course of NAFLD, NASH is an inflammatory state in the liver that contributes to tissue damage and fibrosis formation. Our study shows increased immune cell infiltration in *Pnpla3*$^{148M/M}$ livers, such as CD8^{+} T cells, NK cells, monocytes-derived macrophages and Kupffer cells. The study from Banini et al.[17] found more fibrosis and increased STAT3 activation in PNPLA3 148 M/M overexpressing mice after 16 weeks with a more intense treatment. In our study using PNPLA3 148 M/M knock-in animals, we found higher P-STAT3 activation only after 52 weeks, when severe fibrosis was already present in *Pnpla3*$^{148M/M}$ livers.

Consistent with these findings, the pattern of genes specifically found in the *Pnpla3*$^{148M/M}$ livers link increased inflammation with fibrosis after HFD. In *Pnpla3*$^{148M/M}$ animals, higher *Ephb2* was expressed by HSCs and likely promotes higher levels of *Ccl2* expression. In cooperation with *Ccr2*, more macrophages may be recruited into the liver which in turn regulate the expression of *Ephb2*.[28,29] Besides, earlier studies showed that *Pilrα* reduces macrophage infiltration, while in *Pnpla3*$^{148M/M}$ livers its expression was downregulated indicating that this regulation might be involved in controlling a stronger influx of macrophages into these livers.[31] Eventually, macrophages expressed more Osteopontin which is a biomarker for liver damage. An earlier study provided evidence that Osteopontin could induce fibrosis by triggering ductular response.[43] Taken together, the PNPLA3 I148M genotype supports expression of a gene cluster involved in monocyte-/Kupffer cell-derived inflammation, fibrosis and an increased ductular response in obese animals.

4.1 | Conclusion

Our findings provide long-term data on NAFLD progression in a *Pnpla3*$^{148M/M}$ mouse model which mimics human liver disease. *Pnpla3*$^{148M/M}$ mice showed increased liver damage, cell death and proliferation, inflammation, fibrosis and microbiome changes compared to *Pnpla3*^{WT} mice. An additional set of genes were identified, triggering a more pronounced inflammatory response by activating macrophages and Kupffer cells associated with stronger fibrosis progression.

ACKNOWLEDGEMENTS

We thank Dr. Maria Villar-Fernandez, Katharina Derksen, Carolin Drenda and Hue Kaestel for valuable support concerning the RNA-Seq analysis.

FUNDING INFORMATION

This study was supported by the German Research Foundation CRC1382 (Project-ID 403224013) to MH and CT, as well as DFG HA 7246/2–1 and Tr 285/10–2. The BMBF Knowledge Platform on Food, Diet, Intestinal Microbiomics and Human Health to C.T.

CONFLICT OF INTEREST STATEMENT

There are no potential conflicts (financial, professional, or personal) that are relevant to the manuscript. All authors had access to the study data and had reviewed and approved the final manuscript.

ORCID

Hanns-Ulrich Marschall https://orcid.org/0000-0001-7347-3085
Christian Trautwein https://orcid.org/0000-0003-2762-8247

REFERENCES

1. Dongiovanni P, Donati B, Fares R, et al. PNPLA3 I148M polymorphism and progressive liver disease. *World J Gastroenterol*. 2013;19(41):6969-6978.
2. Valenti L, Al-Serri A, Daly AK, et al. Homozygosity for the patatin-like phospholipase-3/adiponutrin I148M polymorphism influences liver fibrosis in patients with nonalcoholic fatty liver disease. *Hepatology*. 2010;51(4):1209-1217.
3. Wobser H, Dorn C, Weiss TS, et al. Lipid accumulation in hepatocytes induces fibrogenic activation of hepatic stellate cells. *Cell Res*. 2009;19(8):996-1005.
4. Li JZ, Huang Y, Karaman R, et al. Chronic overexpression of PNPLA3I148M in mouse liver causes hepatic steatosis. *J Clin Invest*. 2012;122(11):4130-4144.
5. Mancina RM, Matikainen N, Maglio C, et al. Paradoxical dissociation between hepatic fat content and de novo lipogenesis due to PNPLA3 sequence variant. *J Clin Endocrinol Metab*. 2015;100(5):E821-E825.
6. Huang Y, Cohen JC, Hobbs HH. Expression and characterization of a PNPLA3 protein isoform (I148M) associated with nonalcoholic fatty liver disease. *J Biol Chem*. 2011;286(43):37085-37093.
7. Pingitore P, Pirazzi C, Mancina RM, et al. Recombinant PNPLA3 protein shows triglyceride hydrolase activity and its I148M mutation results in loss of function. *Biochim Biophys Acta*. 2014;1841(4):574-580.
8. Wang Y, Kory N, BasuRay S, Cohen JC, Hobbs HH. PNPLA3, CGI-58, and inhibition of hepatic triglyceride hydrolysis in mice. *Hepatology*. 2019;69(6):2427-2441.
9. Pingitore P, Dongiovanni P, Motta BM, et al. PNPLA3 overexpression results in reduction of proteins predisposing to fibrosis. *Hum Mol Genet*. 2016;25(23):5212-5222.
10. Bruschi FV, Claudel T, Tardelli M, et al. The PNPLA3 I148M variant modulates the fibrogenic phenotype of human hepatic stellate cells. *Hepatology*. 2017;65(6):1875-1890.
11. Krenkel O, Tacke F. Liver macrophages in tissue homeostasis and disease. *Nat Rev Immunol*. 2017;17(5):306-321.
12. Stender S, Kozlitina J, Nordestgaard BG, Tybjærg-Hansen A, Hobbs HH, Cohen JC. Adiposity amplifies the genetic risk of fatty liver disease conferred by multiple loci. *Nat Genet*. 2017;49(6):842-847.

13. Mangge H, Baumgartner BG, Zelzer S, et al. Patatin-like phospholipase 3 (rs738409) gene polymorphism is associated with increased liver enzymes in obese adolescents and metabolic syndrome in all ages. *Aliment Pharmacol Ther*. 2015;42(1):99-105.
14. Valenzuela DM, Murphy AJ, Frendewey D, et al. High-throughput engineering of the mouse genome coupled with high-resolution expression analysis. *Nat Biotechnol*. 2003;21(6):652-659.
15. Smagris E, BasuRay S, Li J, et al. Pnpla3I148M knockin mice accumulate PNPLA3 on lipid droplets and develop hepatic steatosis. *Hepatology*. 2015;61(1):108-118.
16. Ghallab A, Myllys M, Friebel A, et al. Spatio-temporal multiscale analysis of Western diet-fed mice reveals a translationally relevant sequence of events during NAFLD progression. *Cell*. 2021;10(10):2516.
17. Banini BA, Kumar DP, Cazanave S, et al. Identification of a metabolic, transcriptomic, and molecular signature of Patatin-like phospholipase domain containing 3-mediated acceleration of steatohepatitis. *Hepatology*. 2021;73(4):1290-1306.
18. Park J, Zhao Y, Zhang F, et al. IL-6/STAT3 axis dictates the PNPLA3-mediated susceptibility to non-alcoholic fatty liver disease. *J Hepatol*. 2023;78(1):45-56.
19. Cubero FJ, Mohamed MR, Woitok MM, et al. Loss of c-Jun N-terminal kinase 1 and 2 function in liver epithelial cells triggers biliary Hyperproliferation resembling Cholangiocarcinoma. *Hepatol Commun*. 2020;4(6):834-851.
20. Cast A, Kumbaji M, D'Souza A, et al. Liver proliferation is an essential driver of fibrosis in mouse models of nonalcoholic fatty liver disease. *Hepatol Commun*. 2019;3(8):1036-1049.
21. Vansaun MN, Mendonsa AM, Lee GD. Hepatocellular proliferation correlates with inflammatory cell and cytokine changes in a murine model of nonalchoholic fatty liver disease. *PLoS ONE*. 2013;8(9):e73054.
22. Sato K, Marzioni M, Meng F, Francis H, Glaser S, Alpini G. Ductular reaction in liver diseases: pathological mechanisms and translational significances. *Hepatology*. 2019;69(1):420-430.
23. Oliver P, Caimari A, Díaz-Rúa R, Palou A. Diet-induced obesity affects expression of adiponutrin/PNPLA3 and adipose triglyceride lipase, two members of the same family. *Int J Obes (Lond)*. 2012;36(2):225-232.
24. Bibbò S, Ianiro G, Dore MP, Simonelli C, Newton EE, Cammarota G. Gut microbiota as a driver of inflammation in nonalcoholic fatty liver disease. *Mediators Inflamm*. 2018;2018:9321643.
25. Seki E, De Minicis S, Gwak GY, et al. CCR1 and CCR5 promote hepatic fibrosis in mice. *J Clin Invest*. 2009;119(7):1858-1870.
26. Bukong TN, Maurice SB, Chahal B, Schaeffer DF, Winwood PJ. Versican: a novel modulator of hepatic fibrosis. *Lab Invest*. 2016;96(3):361-374.
27. Cruz-Munoz M-E, Dong Z, Shi X, Zhang S, Veillette A. Influence of CRACC, a SLAM family receptor coupled to the adaptor EAT-2, on natural killer cell function. *Nat Immunol*. 2009;10(3):297-305.
28. Mimche PN, Brady LM, Bray CF, et al. The receptor tyrosine kinase EphB2 promotes hepatic fibrosis in mice. *Hepatology*. 2015;62(3):900-914.
29. Mimche PN, Lee CM, Mimche SM, et al. EphB2 receptor tyrosine kinase promotes hepatic fibrogenesis in mice via activation of hepatic stellate cells. *Sci Rep*. 2018;8(1):2532.
30. Remmerie A, Martens L, Thoné T, et al. Osteopontin expression identifies a subset of recruited macrophages distinct from Kupffer cells in the fatty liver. *Immunity*. 2020;53(3):641-657.e614.
31. Kohyama M, Matsuoka S, Shida K, et al. Monocyte infiltration into obese and fibrilized tissues is regulated by PILRα. *Eur J Immunol*. 2016;46(5):1214-1223.
32. Romeo S, Kozlitina J, Xing C, et al. Genetic variation in PNPLA3 confers susceptibility to nonalcoholic fatty liver disease. *Nat Genet*. 2008;40(12):1461-1465.
33. Wilson AS, Koller KR, Ramaboli MC, et al. Diet and the human gut microbiome: an international review. *Dig Dis Sci*. 2020;65(3):723-740.
34. Kim KA, Gu W, Lee IA, Joh EH, Kim DH. High fat diet-induced gut microbiota exacerbates inflammation and obesity in mice via the TLR4 signaling pathway. *PLoS ONE*. 2012;7(10):e47713.
35. Le Roy T, Moens de Hase E, Van Hul M, et al. Dysosmobacter welbionis is a newly isolated human commensal bacterium preventing diet-induced obesity and metabolic disorders in mice. *Gut*. 2022;71(3):534-543.
36. Mouzaki M, Wang AY, Bandsma R, et al. Bile acids and dysbiosis in non-alcoholic fatty liver disease. *PLoS ONE*. 2016;11(5):e0151829.
37. Gadd VL, Skoien R, Powell EE, et al. The portal inflammatory infiltrate and ductular reaction in human nonalcoholic fatty liver disease. *Hepatology*. 2014;59(4):1393-1405.
38. Grimaudo S, Pipitone RM, Pennisi G, et al. Association between PNPLA3 rs738409 C>G variant and liver-related outcomes in patients with nonalcoholic fatty liver disease. *Clin Gastroenterol Hepatol*. 2020;18(4):935-944.e933.
39. Després JP. Is visceral obesity the cause of the metabolic syndrome? *Ann Med*. 2006;38(1):52-63.
40. Zhang W, Huang R, Wang Y, et al. Fat accumulation, liver fibrosis, and metabolic abnormalities in Chinese patients with moderate/severe versus mild hepatic steatosis. *Hepatol Commun*. 2019;3(12):1585-1597.
41. Holland CH, Ramirez Flores RO, Myllys M, et al. Transcriptomic cross-species analysis of chronic liver disease reveals consistent regulation between humans and mice. *Hepatol Commun*. 2022;6(1):161-177.
42. Campos G, Schmidt-Heck W, De Smedt J, et al. Inflammation-associated suppression of metabolic gene networks in acute and chronic liver disease. *Arch Toxicol*. 2020;94(1):205-217.
43. Wang X, Lopategi A, Ge X, et al. Osteopontin induces ductular reaction contributing to liver fibrosis. *Gut*. 2014;63(11):1805-1818.

SUPPORTING INFORMATION

Additional supporting information can be found online in the Supporting Information section at the end of this article.

How to cite this article: Su H, Haque M, Becker S, et al. Long-term hypercaloric diet exacerbates metabolic liver disease in PNPLA3 I148M animals. *Liver Int*. 2023;00:1-15. doi:10.1111/liv.15587